Research Paper

Metal oxychlorides as robust heterogeneous Fenton catalysts for the sonophotocatalytic degradation of 2-nitrophenol

Gamal M.S. ElShafei[a,c,*], A.M. Al-Sabagh[b], F.Z. Yehia[b], C.A. Philip[c], N.A. Moussa[c], Gh. Eshaq[b], A.E. ElMetwally[b]

[a] Taibah University, College of Science, Chemistry Department, AlMadina Almounawara, Saudi Arabia
[b] Egyptian Petroleum Research Institute, Nasr City, Cairo, Egypt
[c] Chemistry Department, Faculty of Science, Ain Shams University, Abbassia, Cairo 11566, Egypt

ARTICLE INFO

ABSTRACT

Metal oxychlorides of Fe, Cu, Bi and Zn were prepared and tested in heterogeneous Fenton degradation of 20 ppm of 2-Nitrophenol (2-NP) in the presence of ultrasonic (US, 20 kHz), ultraviolet (UV, 6 W, λ = 254 nm), and US/UV coupled irradiations. The different experimental conditions including the catalysts dosages, hydrogen peroxide concentration, pH value, temperature, pollutant concentration and irradiation time were optimized and the reusability of the tested metal oxychlorides was investigated as well. The capability of 2-NP degradation follows the order US/UV > UV > US. The rate constant of degradation using sonophotocatalytic system was even higher than the sum of rates of individual systems due to its synergistic performance. Times of 30, 40, 50 and 50 min were respectively needed for Fe, Cu, Bi and Zn oxychlorides to accomplish complete degradation under the experimental conditions of 0.1 gL^{-1} solid, 5 mM H$_2$O$_2$, pH 7 and 25 °C. The rate constant of degradation followed the same order of mentioned metals with values of 0.15, 0.0871, 0.0964, 0.0806, and 0.0738 min^{-1} for Fe, Cu, Bi and Zn oxychlorides, respectively. The mechanism proposed considers a major role of produced hydroxyl radicals while the difference in band gap energy was emphasized in case of Bi and Zn oxychlorides.

1. Introduction

Phenolics are a class of organic compounds that are used immensely in the manufacturing of petrochemicals, pharmaceuticals, preservatives, plastics and agrochemicals. The discharge of these compounds in effluents of the chemical industries has a negative impact on human health and the environment. Among the phenolic compounds, nitrophenols are bio-refractory, inhibitory, toxic, anthropogenic compounds that are utilized greedily in the production of dyes, pharmaceuticals and their intermediates, fine chemicals and pesticides, which are released extensively in the effluents of the above mentioned industries [1,2]. The excessive use of nitrophenols suggests that they are regarded as common pollutants, which should be treated prior to their release into the public wastewater collector system.

Advanced oxidation process (AOP) is one of the most emboldening technologies which has been demonstrated to be efficient and robust in the degradation or mineralization of toxic, inhibitory stable contaminants. This process is capable to generate highly active hydroxyl radical, which is regarded as the second highest robust oxidant after

fluorine [3]. Hydroxyl radicals are capable to react non-selectively without the aid of any chemicals with various contaminants having rate constants in the range of 10^6–10^9 L mol^{-1} s^{-1} [4]. These radicals tend to attack the contaminants molecules either by the hydrogen atom abstraction or the hydroxyl group addition to the double bonds, which in turn give rise to the generation of lower molecular weight intermediates. These intermediates may undergo complete mineralization into water and carbon dioxide [5]. The mineralization of nitrophenols is a quite arduous process when traditional methods are applied, which is attributed to the high stability of nitrophenols molecules.

The use of combined systems such as sono-Fenton or photo-Fenton can enhance the degree of mineralization of organic contaminants [6,7]. However, when the AOP is combined with ultraviolet irradiation, the degradation extent is greatly enhanced due to the generation of great amounts of radicals. This method suffers from several drawbacks accompanied by the continuous operation such as the mass transfer limitations and the adsorption of the pollutant over the catalysts that in turn block the UV active sites. These drawbacks can be handled by the use of ultrasonic irradiation through the acoustic cavitation

phenomena, which cleans up the active sites. Furthermore, the combination of both ultraviolet and ultrasonic irradiation boosts the overall process through the generation of enormous amounts of radicals, which eradicates the drawbacks of the uncombined process [8–10]. Studies have been reported on the degradation of 2-NP using ozonation process under variable dosage of ozone and pH [11–13], the electrochemical degradation using lead oxide/titanium modified electrode [14], the photocatalytic degradation of 2-NP using silver and sulfur co-doped TiO_2 under natural solar light [15]. However, as far as we know there is no report published yet regarding the sonocatalytic or sonophotocatalytic degradation of 2-NP. The use of semiconductors as alternative green photo-catalysts has attracted the attention of scholars in the field of photo-catalysis research [16,17]. Metal oxychloride materials, such as FeOCl, BiOCl, CuOCl and ZnOCl, are class of ternary layered compounds that are characterized by their chemical stability and unique layered structure. The layers of these metal oxychlorides are stacked via van der Waals interaction. The existence of such weak interactions between the layers of metal oxychlorides makes them potential candidates to host organic molecules between their layers [18]. Hosting an organic molecule may lead to a change in the oxidation state ($Fe^{3+} \rightarrow Fe^{2+}$) via charge transfer between the FeOCl matrix and the guest organic molecule [19]. It has been reported that the intercalation of organic molecules into FeOCl layers leaded to the in situ reduction of approximately 25% of ferric ions to ferrous ions [19,20]. It should be pointed out that the presence of a large space between the layers of metal oxychlorides makes them able to polarize the related atoms and orbitals when metal oxychlorides are employed as photocatalysts. Thus, the electron–hole pair can be separated efficiently via the induced dipole, which eventually enhances the photocatalytic activity [21]. Yang et al. [22] have studied the use of iron oxychloride as a Fenton-like catalyst in the oxidative degradation of persistent organic contaminants. They have reported that the remarkable performance of iron oxychloride can be ascribed to the exceptional structural configuration of iron atoms and the reducible electronic features of iron oxychloride.

The purpose of this work is to explore the use of metal oxychloride in the degradation of 2-NP in the presence of ultrasonic (US), ultraviolet (UV), and US/UV coupled irradiations using hydrogen peroxide as an oxidant and present the first report on employing such catalysts in the degradation of 2-NP. In this work, the metal oxychloride catalysts were prepared and characterized using XRD, TEM, SEM, N_2- sorption, FTIR and DRS. The different experimental conditions including the catalysts dosages, hydrogen peroxide concentration, pH value, temperature, pollutant concentration and irradiation time were optimized and the reusability of the tested metal oxychlorides was investigated as well. Furthermore, the synergistic effect of different degradation processes was investigated and the reaction kinetics and degradation mechanism were discussed.

2. Experimental

2.1. Materials

Anhydrous $BiCl_3$, $FeCl_3$, $CuCl_2$, $ZnCl_2$, polyvinylpyrrolidone, PVP, (K30) and ethylene glycol (EG) were purchased from Sigma–Aldrich. Ammonia solution (30%), citric acid monohydrate, hydrochloric acid and ethanol were purchased from Merck.

2.2. Catalysts preparation

2.2.1. Preparation of Fe₂O₃, CuO and ZnO

Fe_2O_3 nanoparticles were prepared by precipitation method. In particular, anhydrous $FeCl_3$ (3.244 g) was dissolved in 80% EG/water mixture (100 ml) at 50 °C under stirring. Next, 25 mL ammonia solution (3 M) was added dropwise under strenuous stirring. The resultant slurry was kept under stirring at 50 °C for 30 min and then aged for 12 h. The precipitate was separated using centrifugation, washed with water and

ethanol and eventually dried at 70 °C for 24 h. The obtained solid was then calcined at 450 °C for 4 h. CuO and ZnO were prepared by the same method using 3.4 g of anhydrous $CuCl_2$ and 2.72 g of anhydrous $ZnCl_2$.

2.2.2. Preparation of FeOCl, CuOCl and ZnOCl

Iron oxychloride was prepared using chemical-vapor transition method as described in [22]. Anhydrous $FeCl_3$ and the prepared Fe_2O_3 nanoparticles were mingled with a molar ratio of 1.3:1. The mingled powder was placed in a glass container that was then evacuated and sealed. The glass container was kept in a muffle furnace at 380 °C for 48 h. The obtained solid was washed with acetone until the unreacted $FeCl_3$ is completely removed and dried at 80 °C for 4 h. Copper oxychloride and zinc oxychloride were prepared with the same method using the corresponding chlorides and oxides.

2.2.3. Preparation of BiOCl

BiOCl nanoparticles were prepared according to the procedure described in [23]. Typically, 22.2 mL of HCl (37%) was added to a certain amount of deionized water. Then, 37.5 mmol of anhydrous bismuth chloride was added to the prepared acidic solution under stirring to ensure a complete dissolution of bismuth chloride. Next, a 250 mL volumetric flask was used to dilute the acidic bismuth chloride solution using deionized water to about 0.15 M and denoted as solution A. Another solution was prepared where 0.04 g of PVP (K30) and 0.76 g of citric acid monohydrate were dissolved in 392 mL deionized water under stirring at 80 °C and denoted as solution B. Thereafter, 8 mL of solution A was added dropwise to solution B for 3 h under vigorous stirring at 80 °C. The resulting precipitate was separated using centrifugation, washed by deionized water and dried at 80 °C overnight.

2.3. Characterization

The purity of the sample phase was validated using XRD analysis on a Philips Powder diffractometer with Cu Kα radiation (λ = 0.154 nm). The patterns were recorded in a range of 2θ = 4–80° with scanning speed $2°θ \, min^{-1}$ and 2 θ step of 0.02°. Scherrer equation was used to estimate the average crystallite size of the samples. FTIR analysis was carried out using Nicolet IS-10 FTIR spectrophotometer with KBr discs. A JEOL JEM-2100 operating at 200 kV was used to obtain TEM micrographs of the samples. A JEOL 5410 operating at 30 kV was used to obtain the SEM micrographs of the samples. Surface texture parameters were obtained by nitrogen sorption using a Quantachrome AS1Win, Instrument at −195.8 °C. Point of zero charge (PZC) of the prepared samples was obtained using mass titration method as described in [24].

2.4. Application of catalyst in US, UV and US/UV induced degradation of 2-NP

A programmable sonicator (Sonics & Materials, Inc., VCX 750) provided with a high grade titanium probe with a diameter of 13 mm that is able to operate unceasingly at a constant frequency (20 kHz) with a changeable output power up to 125 W was utilized to supply the ultrasonic irradiation. The catalytic tests were conducted in 120 mL quartz double jacket reactor and the temperature was thermally regulated using a circulating thermostat. During the entire catalytic testing procedure, the power output of the sonicator was adjusted at 100 W. The probe tip of the sonicator was immersed about 2 cm beneath the surface of the 2-NP solution. To estimate the actual power dissipated (P_{diss}) through the solution, it is assumed that the whole power transmitted to the apparatus is dissipated in form of heat as reported by Lorimer et al. [25]. Supposing that a mass of 110 g water was irradiated, then the P_{diss} is calculated to be 13.86 W. The power density was also calculated and found to be 0.126 W/mL.

A 6 W UV lamp (wavelength 254 nm, 10 cm long and 1 cm diameter) was installed parallel to the quartz double jacket reactor. The

sonicator was turned off when the photo-catalytic experiments were carried out. In addition, the UV lamp was turned off when the sono-catalytic experiments were carried out. Both of the irradiating sources were applied simultaneously during the sono-photo-catalytic experiments. For each catalytic run, sample solution of 110 mL 2-NP solution was poured into the reactor, followed by the addition of certain amount of the catalyst. The catalytic run is initiated by adding the hydrogen peroxide and turning on the sonicator or the UV lamp or both. During the photocatalytic runs, a magnetic stirrer adjusted at a steady 400 rpm was utilized. The pH of the solution was adjusted using sulfuric acid (0.2 M) and sodium hydroxide (0.2 M). When the degradation process was complete, aliquots were instantly centrifuged at 5000 rpm to remove the catalysts. Samples were analyzed using HPLC system equipped with a pump Waters 515, a Waters 2489 UV–vis detector set at 280 nm and a column Waters (X Bridge ™ C18 5 μm 4.6 × 250 mm). A mixture of acetonitrile-Milli-Q water (50:50 by volume) at 1 mL min^{-1} was used as the mobile phase throughout the analysis. TOC content of the samples was determined using a Multi N/C 2100S TOC analyzer (Analytik Jena, Germany).

3. Results and discussion

3.1. Characteristics of the prepared metal oxychlorides

3.1.1. XRD

The XRD patterns of different metal oxychloride are harnessed to validate the structure of the prepared samples as shown in Fig. S1. The XRD pattern of bismuth oxychloride shows peaks at 2Θ = 32.5° (110) that confirm the tetragonal crystal structure of bismuth oxychloride (01-082-0485). There are no any additional peaks observed, which suggests that the prepared bismuth oxychloride nanoparticles are highly pure with a single-phase structure. The XRD pattern of iron oxychloride exhibits an orthorhombic structure, according to the reference pattern of iron oxychloride (01-072-0619). The XRD pattern of copper oxychloride displays a monoclinic structure as implied from the comparison with the reference pattern (01-086-1391). The XRD pattern of zinc oxychloride reveals a rhombohedral structure that concurs with the reference code of zinc oxychloride (01-076-0922). The crystallite size of bismuth oxychloride, zinc oxychloride, iron oxychloride and copper oxychloride were calculated using Scherrer equation and found to be 20 nm, 35 nm, 50 nm and 50 nm, respectively.

3.1.2. TEM

The TEM micrographs of bismuth oxychloride, zinc oxychloride iron oxychloride and copper oxychloride are shown in Fig. S2. The images reveal that the nanoparticles are in ranges of 20–50 nm, 20–35 nm, 20–50 nm and 50–80 nm, respectively, which agree well with the crystallite sizes calculate by Scherrer equation.

3.1.3. SEM

The SEM micrographs of bismuth oxychloride, iron oxychloride, copper oxychloride and zinc oxychloride are shown in Fig. 1. Bismuth oxychloride exhibits a flake-like morphology while iron oxychloride exhibits a stony nature. The SEM micrograph of copper oxychloride indicates platelet-like structure while that of zinc oxychloride appears crusty-like structure.

3.1.4. Nitrogen adsorption–desorption

The N$_2$ sorption isotherms of bismuth oxychloride, copper oxychloride, iron oxychloride and zinc oxychloride are shown in Fig. S3. For the first two samples the isotherm is Type III with hysteresis loop extending till P/P° 0.1. The isotherm type-III is assigned for an almost non-porous material. Its H3 loop which does not exhibit any limiting adsorption at high P/Po is observed with aggregates of plate-like particles giving rise to slit-shaped pores [26] Such characteristics agree well with images of SEM. For the other two samples the isotherm can be

classified as Type II but with different features. The isotherm of Zinc sample displayed a hysteresis loop without lower closure point implying an expanding pore system that is mainly between the crusty particles seen in SEM image. The iron sample displayed an interesting adsorption isotherm that showed the initial knee characterizing the region of monolayer formation; however, the region usually assigned to the start of multilayer formation is characterized by a starting concaved part that followed by the usual uprising due to multilayer formation. The isotherm is further characterized by H3 hysteresis extending down to P/P° = 0.15. These features can be explained based on the presence of a group of narrow but fragile pores that during the formation of monolayer imploded and transformed to open texture, slit shape, on which the formation of limited number of multilayer takes place. In summary the nitrogen adsorption results on the four samples indicate that the confined pore structure is the macro sized inter spaces between the layered shaped particles. BET- equation is used to calculate the values of specific surface area of the samples and data are listed in Table S1 along with the data of total pore volume (Vp) that are taken at P/P° = 0.95. However, these values have to be considered with great caution since the applicability of BET equation with such type of texture is highly questionable.

3.1.5. FTIR

The FTIR spectra of the four oxychlorides samples are shown in Fig. S4. The spectra reveal the bands due to physically adsorbed water in the regions 1650 and 3400–3700 cm^{-1}, besides bands at 524.54 cm^{-1} assigned to Bi−O bond [27], at 487, 508 and 601, cm^{-1} that are assigned to Cu(II)−O vibrations, at 480 cm^{-1}, which is attributed to Fe−O stretching, and at 450 cm^{-1}, which is assigned to Zn-O vibration [28].

3.1.6. Diffuse reflectance spectroscopy

The diffuse reflectance spectra of metal oxychlorides (DRS) are presented in Fig. S5. The absorption edge of FeOCl, CuOCl, ZnOCl and BiOCl occurs at 636, 496, 394 and 365 nm, and the band gap energy was estimated to be 1.95, 2.5, 3.15 and 3.4 eV, respectively. To determine whether the transition character of the sharp edge is direct or indirect, the square and square root of absorption coefficient were plotted against energy as follows [27]:

$$E = h\nu = \frac{1240.8}{\lambda} \tag{1}$$

$$(\alpha h\nu)^2 = \left(\frac{\alpha hc}{\lambda}\right)^{1/r} = \left(\frac{\alpha 1240.8}{\lambda}\right)^{1/r} \tag{2}$$

where **E** is the light energy, **h** is Planck's constant (6.626 × 10^{-34} J s), ν is the light frequency, **c** is the light velocity (3 × 10^8 ms^{-1}), **λ** is the wavelength (nm) and **α** is the absorbance. It is to be noted that **r** = 2 in case of allowed direct transitions and **r** = 1/2 in case of allowed indirect transitions. The plots of the square and square root of absorption coefficient against energy in the absorption edge region for metal oxychlorides are displayed in Fig. 2. For all metal oxychlorides, the square root of absorption coefficient against energy is almost linear while the square of absorption coefficient against energy deviates away from the straight line. Consequently, it can be concluded that the absorption edge of the used metal oxychlorides is caused by an indirect transition.

3.2. Degradation of 2-NP using ultrasonic or photo-heterogeneous Fenton coupling process

3.2.1. Screening the sonolysis & photolysis conditions

Initially, the impact of sonolysis time on the degradation of 2-NP was screened in absence of any extra stimulus to demonstrate the capability of the ultrasonic irradiation (20 kHz) and the obtained data manifest that the extent of degradation after 30 min was only 15% as shown in Fig. S6. The extreme pressure and temperature generated
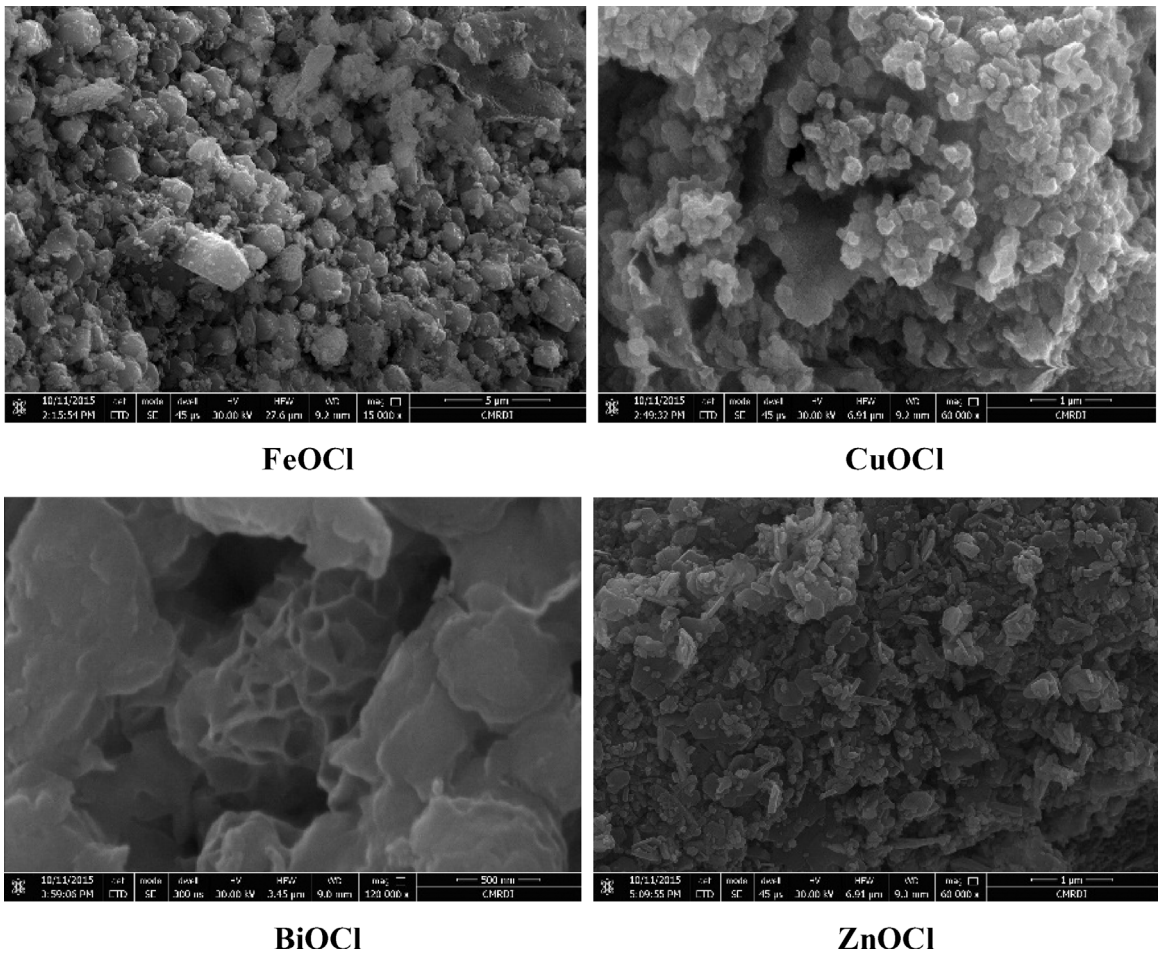
FeOCl

CuOCl

BiOCl

ZnOCl

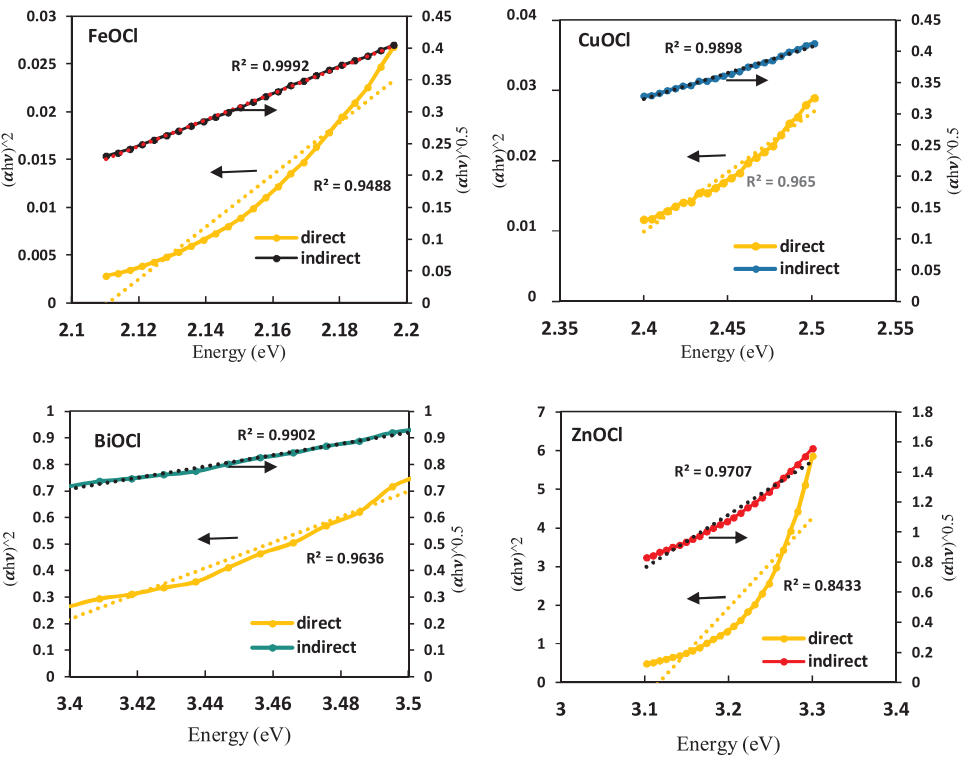**Fig. 1.** SEM images of FeOCl, CuOCl, BiOCl and ZnOCl.

Fig. 2. Plots of $(\alpha h\nu)^2$ vs. energy and $(\alpha h\nu)^{1/2}$ vs. energy in the absorption edge region for FeOCl, CuOCl, BiOCl and ZnOCl.

during the sonolysis of water induces the generation of free radicals such as ·OH and H·, which can generate other reactive oxygen species (ROS) [29,30].

The organic compounds undergo hydroxylation via the generated radicals and furthermore oxidation in presence of oxygen or air [31,32]. However, the rate constant (K) for the reaction of oxygen and H· and that between H· and 2-NP is $2.1 \times 10^{10}\,M^{-1}\,s^{-1}$ and $4.4 \times 10^{10}\,M^{-1}\,s^{-1}$, respectively; while for two hydroxyl radicals combination and for the reaction of ·OH and 2-NP it is 5.2–$6.2 \times 10^{9}\,M^{-1}\,s^{-1}$ and $3.8 \times 10^{9}\,M^{-1}\,s^{-1}$, respectively [4]. The incapability of the sonolysis alone in the degradation of 2-NP is attributed to the significant loss of H· and ·OH even before attacking the 2-NP molecules making the remaining amounts of the radicals insufficient to entirely degrade the molecules of 2-NP.

It is also noted that degradation capability decreases with further increasing the irradiation time, which is ascribed to the degassing of the dissolved gasses. The presence of these gases in the solution promotes the cavitational activity and eventually enhances the degradation capability. The results are consistent with the data reported in [33].

The impact of H_2O_2 concentration on the sonolysis of 2-NP was examined in the range of 5–30 mM as shown in Fig. S6. The results reveal that the degradation extent reaches to about 35% at 20 mM H_2O_2, and beyond this concentration the degradation extent decreases. The leverage of the degradation extent upon the addition of H_2O_2 is ascribed to the enrichment in the generation of the hydroxyl radicals as a result the sonication of H_2O_2. A lower bond energy of 139 kJ mol^{-1} for the oxygen–oxygen bond in hydrogen peroxide than that of oxygen–hydrogen bond (463 kJ mol^{-1}) of water, makes the cleavage of the bond via sonication is much easier [34]. Unfortunately, the enrichment in the generation of the hydroxyl radicals is counteracted by side reactions, which act to scavenge the generated radicals such as the recombination of hydroxyl radicals and the reaction of hydroxyl radical with H_2O_2 ($k = 2.7 \times 10^{7}\,M^{-1}s^{-1}$), which gives rise to hydroperoxyl radical that subsequently reacts with hydroxyl radical ($k = 6 \times 10^{9}\,M^{-1}s^{-1}$) [34]. With regard to the rate constant for the reaction of hydroxyl radical and 2-NP, the inefficiency of coupling the ultrasonic and H_2O_2 to entirely degrade 2-NP can be explained.

The cavitation bubble dynamics is greatly affected by the physical and chemical properties of the solution that are determined by the solution pH. The impact of solution pH on sonolysis of 2-NP was tested in the pH range of 2.7–11 as displayed in Fig. S6. It is clear that the degradation extent reaches its summit (40%) at the strongly acidic pH (2.7) using a very low H_2O_2 concentration of 5 mM, but the degradation extent decreases with increasing the solution pH.

The acidic solution induces the transformation of 2-NP (pka = 7.23) to its molecular form. The dominance of the molecular form in the acidic pH instigates the transformed molecules to be diffused within the gas-liquid zone (reactive region). Moreover, there is a possibility that a little portion of the molecular form evaporates within the cavitation bubble. Accordingly, it can be concluded that the degradation of the

molecular form of 2-NP occurs within both the gas-liquid zone via the generated radicals and the cavitation bubble via pyrolysis. On the other hand, increasing the solution pH towards neutral conditions induces the formation of the ionic form of 2-NP, which is less evaporable. The domination of the ionic form of 2-NP upon increasing the solution pH increases the hydrophilic character of the 2-NP molecules and consequently the molecules tend to reside within the solution bulk away from the cavitation bubbles. Thus, the ionic form of 2-NP molecules will be attacked only by a few amount of hydroxyl radicals at the solution bulk [35]. Consequently, the degradation of the molecules of 2-NP will be only degraded via the radicals generated within the gas–liquid zone. Moreover, the generation of the hydroxyl radicals is retarded at higher pH because the hydrogen peroxide is decomposed into water and $O·_2$ [36,37]. The above mentioned results seem to agree well with the data reported in [17].

To study the impact of photolysis alone, experiments were performed using UV irradiation alone as shown in Fig. S7. The obtained data manifest that the photolysis of 2-NP was insignificant, a degradation extent of only 27% was observed after 1 h of irradiation.

The impact of hydrogen peroxide was tested on the photolysis of 2-NP in the range of 5–30 mM as displayed in Fig. S7. The results show that the degradation extent increases with increasing the concentration of hydrogen peroxide peaking at 20 mM. However, beyond this concentration the degradation extent is inversely proportional to the concentration of hydrogen peroxide. The enhanced degradation capability is attributed to the photolysis of hydrogen peroxide to generate an additional amounts of hydroxyl radicals [38]. However, the suppression of the catalytic activity upon adding an excessive amount of hydrogen peroxide is due to the scavenging phenomenon as mentioned before. It is clear that photolysis has shown superiority over sonolysis in the degradation of 2-NP, which is ascribed to the involvement of reactive species with more diversity than that of sonication system [39,40]. Moreover, the impact of solution pH was tested on the photolysis of 2-NP in the pH range of 2.7–11 as displayed in Fig. S7. It is obvious that the degradation extent reaches its maximum (55%) at the strongly acidic pH (2.7), but the degradation extent decreases with increasing the solution pH.

3.2.2. Optimization of ultrasonic or photo-heterogeneous Fenton coupling process

Silent mode experiments were carried out to probe the capability of the metal oxychlorides in the absence of the ultrasonic irradiation or UV irradiation. The results reveal that on using 0.1 g L^{-1} of the catalysts, 2-NP (20 ppm), 50 mM of H_2O_2, pH 7 and stirring for 1 h, a degradation extent of 25%, 20%, 16% and 15% was observed for FeOCl, CuOCl, ZnOCl, and BiOCl, respectively. The obtained results reveal that the solution upheaval has a limited influence on the degradation extent.

3.2.2.1. Impact of irradiation time.
The efficacy of coupling the metal oxychloride catalysts with the sonolysis system was demonstrated in the
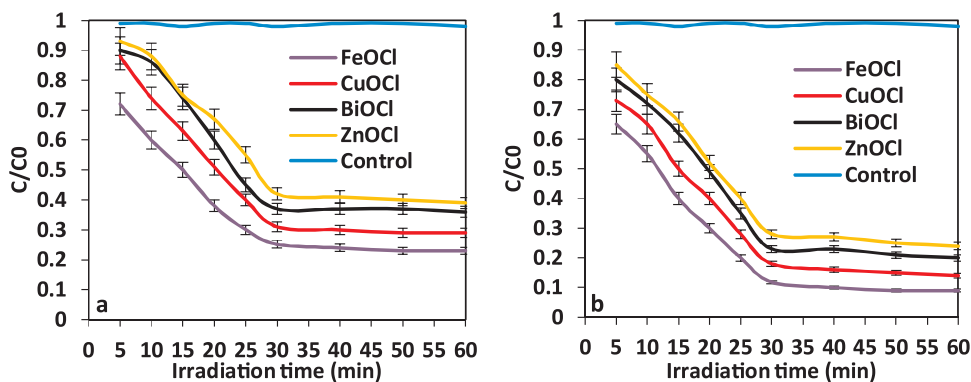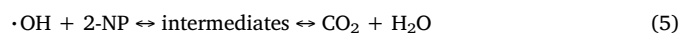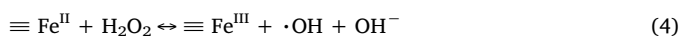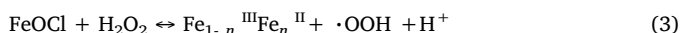

Fig. 3. (a) impact of irradiation time on sonocatalytic degradation of 2-NP. (b) impact of irradiation time on photocatalytic degradation of 2-NP. Reaction conditions:2-NP (20 ppm), catalyst (0.1 g L^{-1}), H_2O_2 (5 mM), pH (7), and 25 °C.

presence of hydrogen peroxide, the impact of irradiation time was tested and the results are displayed in Fig. 3a. Our previous studies have reported the role of ultrasonic irradiation in the enhancement of hydroxyl radical generation in the presence of solid catalysts [35]. The ultrasonic irradiation also acts to increase the number of the active sites and surface area of the catalysts via the turbulence induced by the acoustic cavitation. It is found that the degradation extent increases with increasing the irradiation time and the catalyst's efficiency follows the order FeOCl > CuOCl > BiOCl > ZnOCl. However, in case of the four oxychlorides no complete degradation was obtained even after 60 min of irradiation. The higher efficiency of FeOCl is ascribed to its capability for the generation of huge amounts of hydroxyl radicals. It was reported the capability of α-FeOOH to catalyze the generation of hydroxyl radicals is lower than that of FeOCl by nearly two orders of magnitude [22]. The salient performance of FeOCl is attributed to its intrinsic structure where the plane (020) is satiated with unsaturated iron atoms that is denoted as the polar surface (10.96 at. nm^{-2}) [41]. The presence of hydroxyl groups on the polar surface allow them to perform as active sites that embroiled in diverse process such as anions adsorption, complexation and dissolution [42]. The Fe atom was exposed uniformly over this facet into a linear configuration of $O-Fe-Cl$. The $[Fe-O-Fe]^{4+}$ configuration has shown effectiveness in Fenton reactions induced by photo-radiation using ultrafast laser spectroscopy [22]. Additionally, the ferric ions of FeOCl have high tendency to be reduced to ferrous ions when they react or intercalate with other species. It is to be noted that ferrous ions have a pivotal role in the generation of hydroxyl radicals with a rate higher than those generated over ferric ions by three to four orders of magnitudes. The Lewis base molecules of hydrogen peroxide seem to have more affinity towards the polar facet of iron oxychloride than water [22]. Furthermore, when organic molecules and hydrogen peroxide are absorbed on the catalyst, the charge/electron transfer from hydrogen peroxide to the iron oxychloride leads to a partial reduction during the reaction. Eventually, the degradation of 2-NP takes place via the generated radicals. It should be mentioned that the iron oxychloride is characterized by the facile self-redox features of its iron atoms.

$$FeOCl + H_2O_2 \leftrightarrow Fe_{1-n}{}^{III}Fe_n{}^{II} + \cdot OOH + H^+ \tag{3}$$

$$\equiv Fe^{II} + H_2O_2 \leftrightarrow \equiv Fe^{III} + \cdot OH + OH^- \tag{4}$$

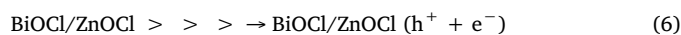$$\cdot OH + 2\text{-NP} \leftrightarrow intermediates \leftrightarrow CO_2 + H_2O \tag{5}$$

It can be concluded that the unrivaled properties of FeOCl and the matchless structural configuration of its atoms are keys that lie behind the exceptional performance of FeOCl in the degradation of 2-NP. Similar pathway can be suggested for CuOCl. We mean that with similar pathway not the same structure but the same attitude for the reaction of Fenton like systems for activating H_2O_2 in advanced oxidation processes. For iron and copper in terms of its reactivity towards H_2O_2 as Fenton catalysts efficiently generate $HO\cdot$ for the oxidation of various organic pollutants in near neutral or neutral aqueous solutions producing OH radicals. Copper shows strikingly similar redox properties like iron. Both the monovalent (Cu^+) and divalent (Cu^{2+}) oxidation states react easily with H_2O_2. However, the superiority of FeOCl over CuOCl in the sonocatalytic degradation of 2-NP depends on the value of the system's redox potential, which is higher in case of Fe (0.771 V) than that of Cu (0.16 V) [35].

In the case of using Semiconductors such as BiOCl and ZnOCl in the sonocatalytic degradation of 2-NP, the radicals are generated by a completely different mechanism. However, the explanation of the proposed mechanism using semiconductors in the ultrasonic assisted degradation of organic contaminants is not yet satisfactory. It was suggested that the sonocatalytic degradation mechanism in the presence of semiconductors occurred via sonoluminescence phenomenon [43]. The ultrasonic irradiation is capable of emitting a light with a relatively wide range of wavelengths. The beams of light with
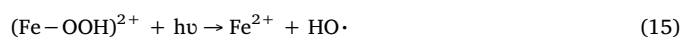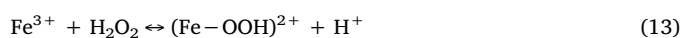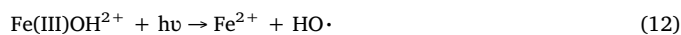
wavelengths lower than 375 nm are capable to excite the electrons of the semiconductors that act as photocatalysts where remarkable amounts of hydroxyl radicals are generated. Furthermore, the extremely high temperature of the localized hotspot generated as a result of the collapse of cavitation bubble is able to bring numerous holes, which in turn produce hydroxyl radicals on the surface of semiconductor catalysts [44]. It can be argued that there is a resemblance between the sonocatalytic and photocatalytic degradation mechanisms when semiconductors are used as catalyst and thus the recombination of electron-hole pairs should be retarded to boost the catalytic performance. However, the production of hydroxyl radicals through this process is apparently less than that in case of iron and copper oxychlorides; therefore both showed lower activities toward 2-NP removal. The values of band gap energy of Bi and Zn oxychlorides control the activity order recorded above. Coupled to this system, the continuous cleaning of the semiconductor catalysts by the ultrasonic irradiation can keep the catalyst reactive for longer periods.

The generation of the hydroxyl radicals using semiconductors in the presence of ultrasonic irradiation can be represented by the following equations [44]:

$$BiOCl/ZnOCl\ >\ >\ >\ \rightarrow BiOCl/ZnOCl\ (h^+ + e^-) \tag{6}$$

$$H_2O\ >\ >\ >\ \rightarrow \cdot OH + H\cdot \tag{7}$$

$$\cdot OH + \cdot OH \rightarrow H_2O_2 \tag{8}$$

$$e^- + O_2 \rightarrow O_2^{\cdot-} \tag{9}$$

$$h+ + H_2O \rightarrow \cdot OH + H^+ \tag{10}$$

$$h^+ + OH^- \rightarrow \cdot OH \tag{11}$$

The indirect transition band gap of both BiOCl and ZnOCl [Section 3.1.6] compels the excited electron to roam a particular k-space distance until it reaches the valence band. Thus, the probability of the electron–hole recombination is efficiently retarded. It can be argued that the indirect transition and loose packed structure of both BiOCl and ZnOCl enhance the retardation of electron–hole recombination that in turn enhance the overall catalytic activity. In spite of the suggestion that the mechanism of radicals generation is the same in case of both BiOCl and ZnOCl, the results reveal that the degradation capability of BiOCl is higher than that of ZnOCl. This is ascribed to the fact that the band gap energy of BiOCl (3.4 eV) is larger than that of ZnOCl (3.15 eV), thus the distance should have traveled by the electron in case of BiOCl is longer than that of ZnOCl. The excitation of a one electron in case of BiOCl takes place from the chlorine' 3p state to the bismuth's 6p state while that in case of ZnOCl takes place from chlorine' 3p state to the zinc 3d.

The coupling of heterogeneous Fenton with the UV irradiation showed increase in the degradation capability with time higher than that obtained in case of coupling with US, with the four oxychlorides following same order, Fig. 3b. Such improved degradation could be attributed to the higher extent of producing hydroxyl radicals. It is clear that the iron oxychloride catalyst has shown supremacy, which may be attributed to the iron recycling phenomenon caused by the photochemical reduction of ferric ions as presented by the following equations [45,46]:

$$Fe(III)OH^{2+} + h\upsilon \rightarrow Fe^{2+} + HO\cdot \tag{12}$$

$$Fe^{3+} + H_2O_2 \leftrightarrow (Fe-OOH)^{2+} + H^+ \tag{13}$$

$$(Fe-OOH)^{2+} \leftrightarrow Fe^{2+} + HO_2\cdot \tag{14}$$

$$(Fe-OOH)^{2+} + h\upsilon \rightarrow Fe^{2+} + HO\cdot \tag{15}$$

$$Fe^{3+}\ HO_2\cdot \rightarrow Fe^{2+} + O_2 + H^+ \tag{16}$$

Similar pathway can be assumed in case of CuOCl, however it exhibits lower efficiency than that of FeOCl because of the redox potential

as discussed before. The photocatalytic degradation mechanism in case of BiOCl and ZnOCl takes place via the classical electron-hole pairs as mentioned above. However, in this case the higher efficiencies are due to direct exposure to a higher flood of photons than that assumed to result as a secondary effect in case of US. Again, in no case a complete degradation was obtained even after 60 min of irradiation.

3.2.2.2. Impact of H₂O₂ concentration. The impact of hydrogen peroxide concentration on sonocatalytic degradation of 2-NP was tested in range of 5–30 mM as displayed in Fig. S8. It is clear that degradation extent of 2-NP increases with increasing the concentration of hydrogen peroxide up to 15 mM reaching 80% and 75%, 68%, and 65% for FeOCl, CuOCl, BiOCl and ZnOCl, respectively. However, beyond this concentration the sonocatalytic degradation capability is retarded with increasing the concentration of hydrogen peroxide. The enhancement of the degradation capability upon increasing the hydrogen peroxide concentration is ascribed to the intensification of the generated hydroxyl radicals. On contrary, the excessive addition of hydrogen peroxide leads to the retardation of degradation capability where the huge amounts of hydroxyl radicals tend to be scavenged by present extra amount of hydrogen peroxide.

The impact of hydrogen peroxide concentration on the photocatalytic degradation of 2-NP was tested in the range of 5–30 mM as displayed in Fig. S9. The added hydrogen peroxide acts as an extra source for the production of reactive species. When ZnOCl and BiOCl are illuminated with UV irradiation, holes (h+) are generated in the valence bands while the conduction band possess electrons (e−). The oxygen acts as electrons consumer where it reacts with electron producing superoxide radical ($O_2^{·-}$). Meanwhile, the hydroxide ion presents on the catalyst surface reacts with holes producing hydroxyl radicals.

Thus, it can be concluded that the presence of significant amount of oxygen is essential for suppressing electron-hole recombination. The hydrogen peroxide acts not only as an extra source for radical generation but also as an electron trap. Hydrogen peroxide reacts with electron in the conduction band and consequently retards the electron-hole recombination process [47].

$$e^- + H_2O_2 \rightarrow OH- + ·OH \qquad (17)$$

$$O_2^{·-} + H_2O_2 \rightarrow ·OH + OH^- + O_2 \qquad (18)$$
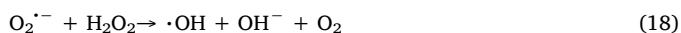
It is obvious that degradation extent of 2-NP increases with increasing the concentration of hydrogen peroxide up to 20 mM resulting in efficiency of 95%, 90%, 85% and 80% for FeOCl, CuOCl, BiOCl and ZnOCl, respectively. The higher efficiency and the positive shift of the upper limit of hydrogen peroxide concentration, relative to US case, imply that the UV irradiation improves the production of hydroxyl radicals more than US that withstand the scavenging effect up to 20 mM of added hydrogen peroxide. However, the suppression of the catalytic activity upon adding an excessive amount of hydrogen peroxide in either case is due to the scavenging phenomenon as described in the following equations:

$$H_2O_2 + ·OH \rightarrow H_2O + HO_2· \qquad (19)$$

$$HO_2· + ·OH \rightarrow H_2O + O_2 \qquad (20)$$

3.2.2.3. Impact of catalyst dosage. The impact of catalysts dosage on degradation of 2-NP was tested using 0.05, 0.1, 0.3, 0.5 and 1.0 g L⁻¹ as displayed in Figs. S8 and S9 . The obtained results reveal that there is an increment in the degradation extent, without change in oxychlorides order, with increasing the catalysts dosage peaking at 0.1 g L⁻¹ in case of US and 0.3 g L⁻¹ in case of UV. However, beyond these catalyst dosages the degradation extent decreases with further increase of the catalyst dosage. The enhanced performance upon increasing the catalyst dosage is ascribed to the availability of a huge number of

active sites on which additional cavitation bubbles are developed that in turn generate an extra amount of hydroxyl radicals (US), and large numbers of pollutant will be adsorbed that will be subjected to a large number of hydroxyl radicals (US/UV). On the other hand, the retarded catalytic performance upon increasing the catalyst dosage (beyond 0.1 g L⁻¹) is because the ultrasonic irradiations are scattered by exaggerated amounts of the catalyst, which also block the ultrasonic waves transmission [48,49]. Moreover, the excessive dosage of catalyst impedes the dispersion of the catalysts by the ultrasonic irradiation and thus the catalyst particles agglomerate leading to the masking of the available active sites. It should be noted that the excessive dosage of catalyst boosts the consumption of the hydroxyl radicals at the solution-bubble interface [50]. On contrary, the photocatalytic activity is inhibited upon increasing the catalyst dosage (beyond 0.3 g L⁻¹) because the UV irradiations are scattered by the catalyst particles, which prohibits the UV irradiations from reaching the neighboring particles [51]. Furthermore, the excessive addition of a catalyst to the solution coerces the catalyst particles to aggregate and consequently the number of the available active sites is reduced. The aggregated particles block the penetration of UV irradiation that in turn reduce the photocatalytic activity [52]. The obtained data seem to be similar to the trends observed for *p*-nitrophenol degradation that is reported in [53]. The negative effect of increasing the catalyst dose is more evident in case of using US than in case of UV.

3.2.2.4. Impact of solution pH. In sonocatalysis, the pollutants distribution within the bulk region and at the liquid-bubble interface can be altered by the solution pH. This phenomenon depends on the nature of the organic pollutant and also the point of zero charge (PZC) of the catalyst added to the system [54] It can be argued that the solution pH has a worthy effect on the surface charge of the catalyst, which is also reflected on the degree of particles aggregation. The impact of solution pH on the sonocatalytic degradation of 2-NP was screened over a wide pH covering the acidic, neutral and basic ranges as displayed in Fig. S8. It is clear that the sonocatalytic performance is favored within the acidic and neutral pH ranges and retarded within the basic range. The impact of solution pH on the sonocatalytic degradation of 2-NP is associated with the ionization states of the pollutant and catalyst surface and also the radical formation rate and the other reactive species [55,56]. It is to be noted that the efficiency of either adsorption or degradation is fostered near the catalyst PZC. The prospect of catalyst dissolution is intensified within the acidic pH ranges that triggers the chances of homogeneous Fenton to take place in the system. But, when the pH value comes close to the neutral range, the prospect of catalyst dissolution is minimized. The PZC of FeOCl, CuOCl, BiOCl, and ZnOCl was measured and found to be 6, 7, 8 and 7 respectively. The charge on the surface of these particles is positive below this PZC value and negative above it. Moreover, the pKa value of 2-NP is 7.23 and thus within neutral ranges the 2-NP molecules are readily attracted, at least have not repelled, to the catalyst surface. On contrary, increasing the pH to the basic ranges force the negatively charged 2-NP molecules to be repelled by the negatively charged particles of the catalyst. Consequently, the molecules of 2-NP will only be degraded by the hydroxyl radicals present in the solution bulk, which is an extremely sluggish process where it is ruled by rate of radical diffusion across the solution bulk. It should be noted that the prompt decomposition of hydrogen peroxide within the basic pH ranges has a great influence on suppressing the degradation capability [35].

The impact of solution pH on the photocatalytic degradation of 2-NP was tested and the data are displayed in Fig. S9. The explanation of the impact of pH on the photocatalytic degradation of organic pollutant is extremely troublesome since there are different mechanisms are assumed such as the direct reduction by means of electrons in the conduction band, the direct oxidation by means of holes in the valence band and finally the hydroxyl radical attack. The degree of contribution of each mechanism relies on the solution pH and substrate nature [57].

The solution pH is capable of modifying the electrical double layer of the liquid- solid interface and thus can influence the adsorption-desorption process and the suppression of electron-hole recombination process.

3.2.2.5. Impact of pollutant initial concentration.

The impact of pollutant initial concentration on its sonocatalytic or photocatalytic degradation was studied using 10, 20, 40 and 80 ppm of 2-NP as displayed in Figs. S8 and S9. The obtained data manifest that the degradation extent has shown its best values at 20 ppm initial concentration of 2-NP. The negative impact of higher concentrations is attributed to the occupancy of the catalyst active sites by a huge numbers of 2-NP molecules that are adsorbed on the catalyst surface, which in turn prohibits the generation of hydroxyl radical on the catalyst surface and consequently reduces the amount of generated radical [58]. The photocatalytic activity has shown similar behavior to that of sonocatalytic activity in relation to pollutant initial concentration. The obtained results are in a good agreement with data reported in [59]. The suppression of photocatalytic capability upon increasing the 2-NP initial concentration is ascribed to the adsorption of the UV irradiation by a huge numbers of 2-NP molecules rather than the catalyst particles. Thus, the concentrated amounts of 2-NP molecules prevent the UV irradiation from reaching the catalyst particles [60]. It can be concluded that applied system is promising in the sonocatalytic or photocatalytic degradation of 2-NP with initial concentration ≤ 20 ppm.

3.2.2.6. Impact of temperature.

The impact of operating temperatures: 15, 25, 35 and 55 °C was tested on the sonocatalytic or photocatalytic degradation of 2-NP as displayed in Figs. S8 and S9. It is clear that, in case of both systems, raising the operational temperature enhances the degradation capability of the system. The operational temperature of sonication system affects the energy of cavitation, cavitation threshold limit and finally the volume of vapor pressure and dissolved gases [8]. Jiang et al. [8] have also argued that the cavitation bubbles may be subjected to a coalescence between each other upon raising the operating temperature and consequently a significant numbers of the collapsing bubbles are lost, which in turn suppress the overall activity. However, this phenomenon can be perturbed when a catalyst is added where the existence of solid particles stimulates the generation of cavitation bubbles on their surface as they act as nuclei for cavitation bubble generation [61]. Thus, the radical species are exceedingly distributed within solution bulk resulting in an increment in the degradation capability [62]. The enhanced degradation capability upon raising the operating temperature agrees well with the results reported in [63]. Furthermore, the elevated operating temperature diminishes the mass transfer of the radical species limitation from the solution bulk, which enhances the reaction rate between the pollutant molecules and radical species at the solid surface. The increment in case of UV system is ascribed to the suppression of the electron-hole recombination process by means of elevated temperature. Moreover, the elevated temperature increases the oxidation rate of organic compounds and thus enhance the degradation capability [64].

3.3. Sonophotocatalytic-assisted heterogeneous Fenton degradation of 2-NP

The coupling of ultrasonic irradiation with photocatalytic process represents one of the neoteric developments targeting the wastewater treatment process. Sonophotocatalytic-assisted heterogeneous Fenton is a reaction where there is a simultaneous irradiation of UV and ultrasonic in the presence of a catalyst and an oxidant such as H_2O_2. The use of such combination enhances the mass transfer of the pollutant molecules from the solution bulk to the catalyst surface. It also helps to disperse the catalyst preventing the aggregation. Moreover, the combined system not only activates the photocatalyst surface but also provides a dual source for the generation of hydroxyl radicals, either by UV or US irradiation. The simultaneous irradiation generates a huge amounts of the radicals that are ready to attack the pollutant molecules, thus this synergistic effect increases the degradation reaction rate. The interpolation of the ultrasonic within the system alleviates the blocking of the catalyst active sites via the incessant cleaning ability provided by the ultrasonic, which also provides supplemental surface area as a result of particles fragmentation and divergence. It is well known that the pollutant adsorption is a rate limiting step for the photocatalytic degradation reaction and consequently the US plays a major role to overcome his obstacle [65]. It can be argued that the coupling of US and UV has the ability to exclude all of the disadvantages that encounter the use of sole processes such as the catalyst fouling and mass transfer limitations [54]. It is assumed that the sonophotocatalytic oxidation mechanism is a hybrid of both photocatalysis and sonocatalysis. The reactivity modes of sonolysis involve the hydroxyl radical oxidation and pyrolytic decomposition that have been discussed in detail in [66,67]. It is to be noted that the hydroxyl radical is considered the main oxidizing species generated by both US and UV irradiation.

The different parameters of sonocatalytic and photocatalytic degradation of 2-NP have been optimized to achieve a maximum performance using least amounts of catalyst and hydrogen peroxide for short period of time. Then, the optimized parameters were applied for the sonophotocatalytic system to foster the catalytic performance and examine the synergy of US and UV. However, from economic point of view, it is highly recommended to conduct the degradation reaction at room temperature to save energy, especially with the moderate efficiencies obtained at room temperature. Furthermore, to emphasize the economic aspect we tested the sonophotocatalytic degradation of 20 ppm of 2-NP at pH = 7 using 5 mM H_2O_2 with 0.1 g L^{-1} of solid catalyst.

The impact of irradiation time of the dual source was tested on sonophotocatalytic degradation of 2-NP (20 ppm), and the results are displayed in Fig. 4a. The obtained data manifest that the degradation extent reaches 100% after 30, 40, 50 and 50 min of dual irradiation for FeOCl, CuOCl, BiOCl and ZnOCl, respectively. The results show that the degradation capability was higher than that of sonocatalytic or
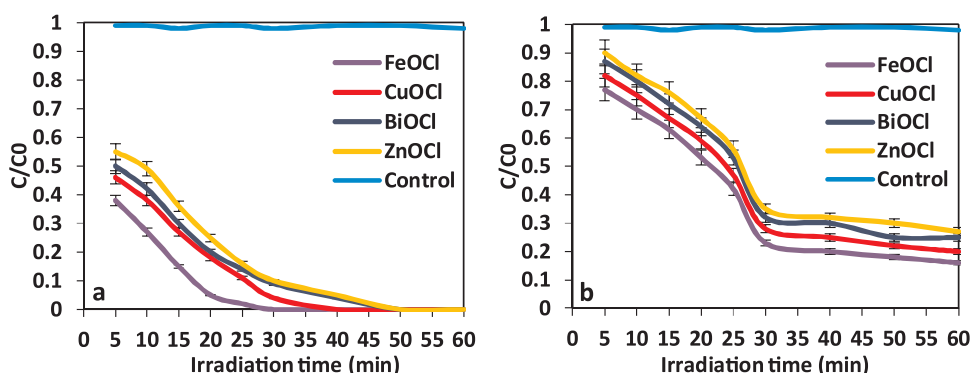

Fig. 4. Sonophotocatalytic degradation of 2-NP. (a) impact of irradiation time. (b) TOC monitoring for sonophotocatalytic degradation of 2-NP. Reaction conditions:2-NP (20 ppm), catalyst (0.1 g L^{-1}), H_2O_2 (5 mM), pH (7), and 25 °C.

Table 1
First order rate constants of the degradation of the 2-NP in the presence of heterogeneous Fenton catalysts.

Catalyst	$K_{US + UV + heterogeneousFenton}$	$k_{UV + heterogeneousFenton}$	$k_{US + heterogeneousFenton}$	Synergy	Synergy (%)
FeOCl	0.15	0.0661	0.0475	0.243	24.3
CuOCl	0.0964	0.0519	0.0361	0.087	8.7
BiOCl	0.0806	0.0423	0.0292	0.1129	11.29
ZnOCl	0.0738	0.037	0.0241	0.172	17.2

photocatalytic degradation by 32% and 18%, respectively.

It is noted that the 2-NP degradation rates using simultaneous irradiations in the presence of metal oxychlorides are greater than the sum of 2-NP degradation rates using sole US or UV irradiations in the presence of metal oxychlorides and thus it exhibits a synergistic effect, Fig. S10. The degradation capability of 2-NP can be arranged as sono-photocatalytic degradation > photocatalytic degradation > sonocatalytic degradation. The first order rate constants can be used to compare the rates of 2-NP degradation that were measured under different operational conditions, Table 1.

There is a possibility for quantifying the synergy as a normalized difference between the rate constants calculated in case of sonophoto-catalysis and the sum of rate constants calculated in case of individual sonocatalysis and photocatalysis, Eq. (21) [51].

$$\text{synergy}(\%) = \frac{k_{\text{sonophotocatalysis}} - (k_{\text{sonocatalysis}} + k_{\text{photocatalysis}})}{k_{\text{sonophotocatalysis}}} X100 \qquad (21)$$

The obtained data are summarized in Table 1, which reveal that synergetic effect caused sonophotocatalytic degradation faster than the other individual process under the same operational conditions. The rate constants of the sonophotocatalysis of 2-NP using the different metal oxychloride catalysts were compared with other sonophotocata-lytic systems that employed different catalysts for degradation of different pollutant as displayed in Table S2. The included results indicate the high impact of synergetic effect in the present study, furthermore it illustrates the superior role of US/UV&heterogeneous Fenton combined system in 2-NP degradation in comparison with the sole using of UV. The use of US solely for 2-NP degradation appears scarce in the literature.

3.4. Catalyst durability

The successive use of a catalyst and also the sustainability of its sonophotocatalytic performance is of a significant solicitude when it is applied on a large scale. To validate the sustainability of the utilized metal oxychlorides, successive runs have been carried out using the generated catalyst. The recovered catalyst is collected after each run and dried to be ready for the next run. It is to be noted that all the sustainability testing runs were performed under the same operating conditions. The obtained data display an insignificant decrease in the sonophotocatalytic performance even after the fourth run as shown in Table S3. The results reveal that the metal oxychlorides catalysts are durable under the defined conditions in this study, and can endure the sonophotocatalytic condition even after the fourth run.

3.5. Mineralization measurement

The mineralization of organic pollutant is of significant concern specially for environmental applications because the persistence of degradation intermediates is even more hazardous than the starting organic compound. Thus, TOC analysis must be carried out to grantee the complete removal of the organic pollutants and their degradation intermediates. The impact of sonophotocatalytic irradiation time was examined on the degree of 2-NP mineralization using the four oxy-chlorides as shown in Fig. 4b. It is clear that the mineralization extent of the sonophotocatalytic system after 60 min reaches 84%, 80%, 78%

and 75% for FeOCl, CuOCl, BiOCl and ZnOCl, respectively, in spite of the fact that the degradation curve in case of the four oxychlorides indicated complete degradation of 2-NP before 60 min. The TOC data validate the efficiency of sonophotocatalytic system in the degradation, but incomplete mineralization of 2-NP can be inferred. After 30 min of irradiation the degradation of 2-NP continues while the change in the TOC values adopt a sluggish decrease up to 60 min. Careful examination of the degradation curves that were collected at 5 min intervals, Fig. 4a, reveal that the degradation profiles are not monotonic implying that the degradation processes proceed via formation of different species. The formed species could be of slower rate of reaction with attacking hydroxyl radicals, and therefore need longer time to be completely disappear.

3.6. Proposed mechanism

The mechanism of 2-NP degradation in presence of iron oxychloride is thought to occur via heterogeneous Fenton. First, the adsorbed hydrogen peroxide molecules on the catalyst surface form a complex with the FeOCl surface ($\equiv Fe^{III}-OH$). Then, an electron transfer reaction leads to the generation of an electronic excited complex ($\equiv Fe^{II} \cdot O_2H$) that dissociates into hydroperoxyl radical and $\equiv Fe^{II}$ [68,69]. Next, hydrogen peroxide reacts with the generated $\equiv Fe^{II}$ to produce $\equiv Fe^{III}$ and hydroxyl radical (Eq. (4)) that is ready to attack the 2-NP molecules.

The catalytic degradation of nitrophenols is reported to take place through two phases, the first one involves the destruction of the aromatic ring (fast step) while the second involves the catalytic oxidation of the aliphatic intermediates (slow step) [70]. Nitrophenols are characterized by the presence of electron-donating group (phenolic $-OH$) and electron-withdrawing group ($-NO_2$). The presence of phenolic $-OH$ group within the 2-NP molecule increases the electron density at para and ortho positions while that of $-NO_2$ group is a meta directing group. The hydroxyl radical is an electrophile that tends to attack the para and ortho position of nitrophenol molecule that are rich in electrons [71]. It has been reported that hydroxyl radical attacked the 2-NP molecule at ortho and para position forming 3-nitrocatechol and 2-ni-trohydroquinone [72].

The degradation pathway of 2-NP using sonophotocatalytic system can be described as illustrated in Scheme S1, where the generated hydroxyl radical attacks the 2-NP molecule to form 3-nitrocatechol (phase1) that is further undergoes ring opening to form carbon dioxide, nitrite and water. Also, the 2-nitrohydroquinone is further oxidized via the hydroxyl radical to form nitrobenzoquinone. Thereafter, the aromatic compound undergoes a ring opening process to produce different aliphatic intermediates. Furthermore, the generation of nitrate ion as an intermediate is attributed to the denitration process of the 2-NP molecule. It has been reported that the concentration of nitrite ions increases and speedily disappears during the degradation of 2-NP [73–75]. The nitrite ions were then oxidized via hydroxyl radicals producing nitrate ions [76]. It must be pointed out that the incessant reduction in TOC values during the sonophotocatalytic degradation of 2-NP manifests the gradual mineralization of the 2-NP molecules. It has been reported that the rate of substrate disappearance is faster than CO_2 generation, which manifested that the degradation of the intermediates is much slower than the initial pollutant molecules [70]. The rapid reduction in the

Table 2
Values of the rate constant of interaction of some compounds with hydroxyl radical [4].

Compound (pH)	Rate constant (L mol^{-1} s^{-1})
Acetate (7)	$7.9–8.5 \times 10^7$
Formate (7)	2.6×10^9
Fumaric acid (4–10.5)	6.0×10^9
Maleic acid (4–10.5)	6.0×10^9
Malonate (6–7)	$6–7 \times 10^8$
Carbon dioxide (4)	$< 1 \times 10^6$
Oxalate (6)	7.7×10^6

TOC values during the initial stages of the reaction can be ascribed to the degradation of the aromatic intermediates while the slow TOC reduction during the later stages can be ascribed to degradation of aliphatic intermediates [77,78]. Table 2 collects values of rate constant of hydroxyl radical interaction with suggested intermediates according to proposed mechanism. The lower values of the rate constants than that of 2-NP could explain the observed non zero values of TOC.

4. Conclusion

In conclusion, the sonophotocatalytic degradation of 2-NP was fulfilled using metal oxychloride as catalysts in the presence of hydrogen peroxide as an oxidant. The employment of metal oxychloride as catalysts propels the degradation capability of the coupled system using the least amount of catalyst and oxidant for a short period of time. Among the tested metal oxychloride, iron oxychloride exhibited superiority over the other tested catalysts. The results reveal that the metal oxychlorides catalysts are durable and can endure the sonophotocatalytic condition even after the fourth run. The obtained results revealed that the 2-NP degradation rates using simultaneous irradiations in the presence of metal oxychlorides were greater than the sum of 2-NP degradation rates using sole US or UV irradiations in the presence of metal oxychlorides and thus it exhibits a synergistic effect. Degradation proceeded via attack by produced hydroxyl radicals resulting in the formation of intermediates that react with hydroxyl radicals with slower rates. According to the values of TOC recorded at the end of degradation, these intermediates could be totally mineralized under more drastic conditions of higher oxidant concentration, longer time of irradiation, and/or higher US power.

Appendix A. Supplementary data

Supplementary data associated with this article can be found, in the online version, at http://dx.doi.org/10.1016/j.apcatb.2017.11.015.

References

[1] V. Kavitha, K. Palanivelu, J. Photochem. Photobiol. A Chem. 170 (2005) 83–95.
[2] F.Z. Yehia, G. Eshaq, A.E. ElMetwally, Egypt. J. Pet. 25 (2016) 239–245.
[3] R. Andreozzi, V. Caprio, A. Insola, R. Marotta, Catal. Today 53 (1999) 51–59.
[4] G.V. Buxton, C.L. Greenstock, W.P. Helman, A.B. Ross, J. Phys. Chem. Ref. Data 17 (1988) 513–886.
[5] M. Mohajerani, M. Mehrvar, F. Ein-Mozaffari, Int. J. Eng. 3 (2009) 120–146.
[6] P.R. Gogate, Ultrason. Sonochem. 15 (2008) 1–15.
[7] M.V. Bagal, P.R. Gogate, Ultrason. Sonochem. 21 (2014) 1–14.
[8] F. Méndez-Arriaga, R. Torres-Palma, C. Pétrier, S. Esplugas, J. Gimenez, C. Pulgarin, Water Res. 42 (2008) 4243–4248.
[9] Y. Suzuki, H. Arakawa, A. Maezawa, S. Uchida, Int. J. Photoenergy 1 (1999) 60–64.
[10] C. Ao, S. Lee, J. Yu, J. Xu, Appl. Catal. B Environ. 54 (2004) 41–50.
[11] A. Shokri, Russ. J. Appl. Chem. 88 (2015) 2038–2043.
[12] M. Kuosa, A. Laari, A. Solonen, H. Haario, J. Kallas, Chem. Eng. Sci. 64 (2009) 2332–2342.
[13] L. Gu, X. Zhang, L. Lei, Ind. Eng. Chem. Res. 47 (2008) 6809–6815.
[14] F.R. Zaggout, N.A. Ghalwa, J. Environ. Manage. 86 (2008) 291–296.
[15] M. Feilizadeh, A. Delparish, S.T. Bararpour, H.A. Najafabadi, S.M.E. Zakeri, M. Vossoughi, Water Sci. Technol. 72 (2015) 339–346.
[16] M.A. Ischay, M.E. Anzovino, J. Du, T.P. Yoon, J. Am. Chem. Soc. 130 (2008) 12886–12887.
[17] K.P. Mishra, P.R. Gogate, Ultrason. Sonochem. 18 (2011) 739–744.
[18] R. Herber, R. Cassell, Inorg. Chem. 21 (1982) 3713–3716.
[19] I. Jarrige, Y. Cai, S. Shieh, H. Ishii, N. Hiraoka, S. Karna, W.-H. Li, Phys. Rev. B 82 (2010) 165121.
[20] S. Hwang, W.-H. Li, K. Lee, J. Lynn, C.-G. Wu, Phys. Rev. B 62 (2000) 14157.
[21] X. Xiao, W.-D. Zhang, Rsc. Adv. 1 (2011) 1099–1105.
[22] X.-j. Yang, X.-m. Xu, J. Xu, Y.-f. Han, J. Am. Chem. Soc. 135 (2013) 16058–16061.
[23] K. Zhang, D. Zhang, J. Liu, K. Ren, H. Luo, Y. Peng, G. Li, X. Yu, CrystEngComm 14 (2012) 700–707.
[24] A.S. Franca, L.S. Oliveira, M.E. Ferreira, Desalination 249 (2009) 267–272.
[25] J. Lorimer, T. Mason, K. Fiddy, Ultrasonics 29 (1991) 338–343.
[26] A. Bhunia, I. Boldog, A. Möller, C. Janiak, J. Mater. Chem. A 1 (2013) 14990–14999.
[27] K.-L. Zhang, C.-M. Liu, F.-Q. Huang, C. Zheng, W.-D. Wang, Appl. Catal. B Environ. 68 (2006) 125–129.
[28] J. Singh, P. Kumar, K.S. Hui, K. Hui, K. Ramam, R. Tiwari, O. Srivastava, CrystEngComm 14 (2012) 5898–5904.
[29] K.S. Suslick, L.A. Crum, M. Crocker, M.J. Crocker John Wiley & Sons (1997) 271-282.
[30] C. Petrier, M.-F. Lamy, A. Francony, A. Benahcene, B. David, V. Renaudin, N. Gondrexon, J. Phys. Chem. 98 (1994) 10514–10520.
[31] A. Henglein, Ultrason. Sonochem. 2 (1995) S115–S121.
[32] C. Sonntag, J. Chem. Soc. Perkin Trans. 2 (1999) 1129–1136.
[33] R. Chand, N.H. Ince, P.R. Gogate, D.H. Bremner, Sep. Purif. Technol. 67 (2009) 103–109.
[34] A. Mehrdad, R. Hashemzadeh, Ultrason. Sonochem. 17 (2010) 168–172.
[35] G.M. ElShafei, F. Yehia, O. Dimitry, A. Badawi, G. Eshaq, Ultrason. Sonochem. 21 (2014) 1358–1365.
[36] C. Sahunin, J. Kaewboran, M. Hunsom, Reactions 22 (2006) 23.
[37] M. Sivakumar, P.A. Tatake, A.B. Pandit, Chem. Eng. J. 85 (2002) 327–338.
[38] F.J. Beltran, Chemical Degradation Methods for Wastes and Pollutants: Environmental and Industrial Applications, CRC Press, 2003.
[39] A.H. Mahvi, A. Maleki, M. Alimohamadi, A. Ghasri, Korean J. Chem. Eng. 24 (2007) 79–82.
[40] E. Naffrechoux, S. Chanoux, C. Petrier, J. Suptil, Ultrason. Sonochem. 7 (2000) 255–259.
[41] C.M. Eggleston, A.G. Stack, K.M. Rosso, S.R. Higgins, A.M. Bice, S.W. Boese, R.D. Pribyl, J.J. Nichols, Geochim. Cosmochim. Acta 67 (2003) 985–1000.
[42] M.A. Barteau, Chem. Rev. 96 (1996) 1413–1430.
[43] N. Shimizu, C. Ogino, M.F. Dadjour, T. Murata, Ultrason. Sonochem. 14 (2007) 184–190.
[44] J. Wang, Z. Jiang, L. Zhang, P. Kang, Y. Xie, Y. Lv, R. Xu, X. Zhang, Ultrason. Sonochem. 16 (2009) 225–231.
[45] C.C. Amorim, M.M. Leão, R.F. Moreira, J.D. Fabris, A.B. Henriques, Chem. Eng. J. 224 (2013) 59–66.
[46] M. Tokumura, R. Morito, R. Hatayama, Y. Kawase, Appl. Catal. B Environ. 106 (2011) 565–576.
[47] S. Malato, J. Blanco, M. Maldonado, P. Fernández-Ibáñez, A. Campos, Appl. Catal. B Environ. 28 (2000) 163–174.
[48] Y.L. Pang, A.Z. Abdullah, Appl. Catal. B Environ. 129 (2013) 473–481.
[49] Y.L. Pang, A.Z. Abdullah, S. Bhatia, Desalination 277 (2011) 1–14.
[50] Z. Eren, N.H. Ince, J. Hazard. Mater. 177 (2010) 1019–1024.
[51] A. Verma, H. Kaur, D. Dixit, Arch. Environ. Prot. 39 (2013) 17–28.
[52] K. Jyothi, S. Yesodharan, E. Yesodharan, Curr. Sci. 109 (2015) 00113891.
[53] N. San, A. Hatipoğlu, G. Koçtürk, Z. Çınar, J. Photochem. Photobiol. A Chem. 146 (2002) 189–197.
[54] P.R. Gogate, A.B. Pandit, AIChE J. 50 (2004) 1051–1079.
[55] E. Hapeshi, A. Achilleos, M. Vasquez, C. Michael, N. Xekoukoulotakis, D. Mantzavinos, D. Kassinos, Water Res. 44 (2010) 1737–1746.
[56] I. Michael, E. Hapeshi, C. Michael, D. Fatta-Kassinos, Water Res. 44 (2010) 5450–5462.
[57] W. Tang, Z. Zhang, H. An, M. Quintana, D. Torres, Environ. Technol. 18 (1997) 1–12.
[58] A. Khataee, R.D.C. Soltani, A. Karimi, S.W. Joo, Ultrason. Sonochem. 23 (2015) 219–230.
[59] M. Mrowetz, C. Pirola, E. Selli, Ultrason. Sonochem. 10 (2003) 247–254.
[60] N. Daneshvar, D. Salari, A. Khataee, J. Photochem. Photobiol. A Chem. 157 (2003) 111–116.
[61] M.A. Behnajady, N. Modirshahla, M. Shokri, B. Vahid, Ultrason. Sonochem. 15 (2008) 1009–1014.
[62] E.V. Rokhina, E.A. Golovina, H. van As, J. Virkutyte, Chemosphere 77 (2009) 148–150.
[63] M.H. Entezari, A. Heshmati, A. Sarafraz-yazdi, Ultrason. Sonochem. 12 (2005) 137–141.
[64] L. Karimi, S. Zohoori, M.E. Yazdanshenas, J. Saudi Chem. Soc. 18 (2014) 581–588.
[65] Y.G. Adewuyi, Environ. Sci. Technol. 39 (2005) 8557–8570.
[66] Y.G. Adewuyi, Ind. Eng. Chem. Res. 40 (2001) 4681–4715.
[67] Y.G. Adewuyi, Environ. Sci. Technol. 39 (2005) 3409–3420.
[68] A.M. Al-Sabagh, F.Z. Yehia, G. Eshaq, A.E. ElMetwally, A.C.S. Sustainable Chem. Eng. (2017).
[69] S.-S. Lin, M.D. Gurol, Environ. Sci. Technol. 32 (1998) 1417–1423.
[70] A. Di Paola, V. Augugliaro, L. Palmisano, G. Pantaleo, E. Savinov, J. Photochem. Photobiol. A Chem. 155 (2003) 207–214.
[71] F.A. Carey, R.J. Sundberg, Advanced Organic Chemistry: Part A: Structure and Mechanisms, Springer Science & Business Media, 2007.
[72] A. Alif, J.-F. Pilichowski, P. Boule, J. Photochem. Photobiol. A Chem. 59 (1991)

209–219.

[73] M.S. Dieckmann, K.A. Gray, Water Res. 30 (1996) 1169–1183.

[74] K.-h. Wang, Y.-h. Hsieh, L.-j. Chen, J. Hazard. Mater. 59 (1998) 251–260.

[75] V. Maurino, C. Minero, E. Pelizzetti, P. Piccinini, N. Serpone, H. Hidaka, J. Photochem. Photobiol. A Chem. 109 (1997) 171–176.

[76] Y. Hori, A. Nakatsu, S. Suzuki, Chem. Lett. 14 (1985) 1429–1432.

[77] J. Kiwi, C. Pulgarin, P. Peringer, Appl. Catal. B Environ. 3 (1994) 335–350.

[78] C. Minero, E. Pelizzetti, P. Piccinini, M. Vincenti, Chemosphere 28 (1994) 1229–1244.